Coatingless, tunable finesse interferometer for gravitational wave detection

G. Cella* and A. Giazotto†

I.N.F.N. Pisa, Largo Bruno Pontecorvo 1, 56100 Pisa, Italy

(Received 21 June 2006; published 25 August 2006)

Future generation gravitational wave interferometric detectors will require a strong reduction of thermal noise, and will be limited by quantum fluctuations of laser light, namely, shot noise and radiation pressure noise. One of the factors which currently constrain the thermal noise performances of this kind of instruments is the dissipation introduced by the optical coating of the mirrors. In a recent article Braginsky and Vyatchanin proposed to reduce the contribution of thermoelastic noise in the coating building an optical cavity with corner reflectors instead of spherical mirrors. In this work we study a solution which, avoiding completely any kind of coating, allows for injection and extraction of light. We discuss the proposed optical scheme, evaluating the expected thermal noise performances.

DOI: 10.1103/PhysRevD.74.042001 PACS numbers: 04.80.Nn, 42.15.Eq, 43.50.+y

I. INTRODUCTION AND MOTIVATIONS

In order to obtain the high resolutions needed in the optical detectors of gravitational waves high reflectivities of optical elements are required. The use of multilayer dielectric coating on mirrors allows today to obtain state of the art values of $R \simeq 1 - 10^{-6}$. The price to pay is an increase of thermal noise induced both by the large thermal expansion coefficient of the coating's material and by the reduction of the mirror's mechanical Q factor [1]. For a given elastic mode the quality factor is usually related to the one of an uncoated mirror by [2–4]

$$Q^{-1} = Q^{-1}_{\text{uncoated}} + \phi \frac{E_{\text{coat}}}{E_{\text{total}}}, \tag{1}$$

where ϕ is the coating's loss angle and E_{coat}, E_{total} are the energies stored in the coating and in the bulk. Values of ϕ for typical coating's materials have been experimentally measured and found to be of the order of few 10^{-4}, to be compared with bulk's ones of the order 10^{-8}. Recent measurements suggest that coating losses does not decrease at low temperature [5].

The search of materials with better performances is currently an active field of research. We think it is worth to try to investigate alternative solutions, which should be able to design highly reflecting optical elements without coatings. The proposal of Braginsky and Vyatchanin ([6], B&V from now on) is based on the total reflection of light from an interface between a dielectric and the vacuum, which is possible when the light impinges from the dielectric's side at a large enough incidence angle, $\sin\theta_i > n^{-1}$. In B&V the authors investigate the properties of an optical cavity with corner reflectors used as mirrors. Optically this configuration is up to some extent equivalent to a plane mirror, and in order to obtain a stable cavity the corner reflectors are supplemented by a lens. As the curvature of this lens is not matched to the resonating mode inside the cavity an anti reflective coating is needed in order to avoid the generation of optical losses.

In this paper we elaborate this proposal to obtain a solution which does not need in principle any kind of coating, and we give a specific solution for the injection of the laser light and its extraction.

In order to avoid anti reflective coatings we propose to change the shape of the reflectors. In our approach the optical stabilization of the cavity is obtained giving an appropriate curvature to the back surface of the reflectors. We will show that in this case the reflector is optically equivalent to a curved mirror, so no additional optics is needed for stabilization.

To avoid spurious reflections from the front surface of our ''coatingless mirror'' (CM) we match it to the cavity mode. The idea is not to avoid the back reflection from the front surface, which is not possible in a simple interface without coating, but to couple the reflected light to the same mode which is resonating. In this way the reflector can be seen as a single mirror, modulo a phase factor in the reflected light which depends on its internal geometry.

A problem with this kind of all reflective cavity is that it is not obvious how to feed the light of the external source inside. We thought about several possible solutions.

A possibility is to couple the evanescent wave which is present on the back of the reflector to another dielectric medium, so that it becomes possible to put light inside the cavity using tunnel effect. This is an interesting possibility in our opinion, worth of further investigation. It allows for example to tune the coupling between the cavity and the external world, so that the finesse of the cavity can be changed up to some extent. But it has also some drawbacks, for example, it seems quite difficult to stabilize with high accuracy the relative position of the reflector and of the ausiliary dielectric.

Another idea is to realize with a piece of dielectric material a coupler between the external input and output modes and the internal ones. Of course it is very easy to do that just with a slab of a dielectric material. The problem is that, in order to obtain high finesse cavities, we need this

*Electronic address: giancarlo.cella@pi.infn.it
†Electronic address: adalberto.giazotto@pi.infn.it

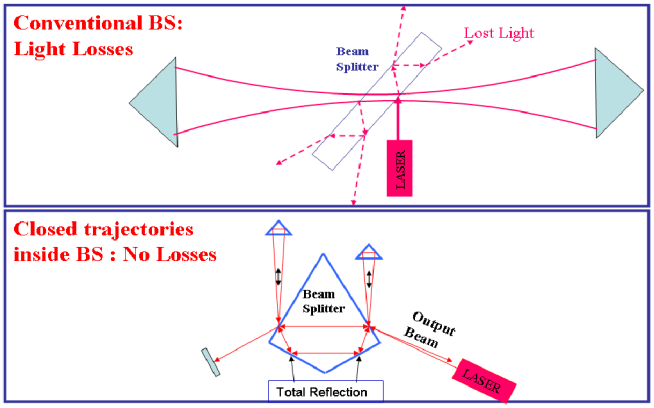

FIG. 1 (color online). A possibility for coupling a coatingless cavity with the laser source and the readout. The schematic idea is shown in the upper diagram. With a naive implementation spurious modes are generated in the general case. In the lower figure we show a more careful implementation which avoids losses.

coupling to be small, which means that the transmission coefficient of the slab must be small. The mimimum transmission coefficient obtainable with a dielectric slab at normal incidence is given by

$$t_{\min} = \frac{2n}{1+n^2}, \tag{2}$$

where n is the refraction index of the material. For reasonable values of n this is not much smaller than 1, for example $n_{Si} \simeq 3.4$ which means $t_{\min,Si} \simeq 0.54$.

From these considerations we argue that using a dielectric at normal incidence is not a good option. But in order to find a solution without a normal incidence angle we need to solve two kind of problems. First of all we expect a proliferation of spurious reflected beams inside the dielectric, which must be avoided. The second issue is that, in the usual setup, the cavity mode should be reflected back in itself and it seems that this is not possible without normal incidence.

We found that it is possible to introduce a prism which is traversed by the resonant beam inside the cavity in such a way to split a fraction of it externally. A schematic diagram for this solution is depicted in Fig. 1. In order to avoid internal and external spurious reflections the geometry of this prism should be accurately tuned. By lowering the reflectivity of the prism it is possible to tune the cavity finesse. But in order to avoid light losses we need to satisfy additional geometrical constraints. Also, we must keep the prism well aligned and this makes a practical scheme quite complicated.

A simpler approach avoids the introduction of the prism inside the cavity. It consist in changing the shape of one of the two reflectors, which acts now not only as a mirror but also as a coupler.

Possibilities of this kind can be derived from the general scheme shown schematically in Fig. 2 as we will explain in

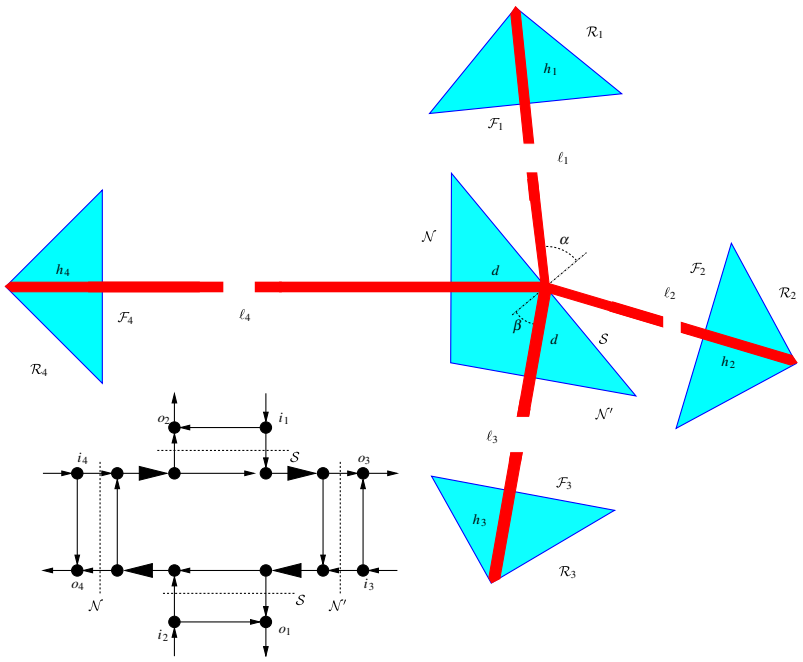

FIG. 2 (color online). The basic optical setup for a coatingless resonant cavity. Each triangle is the section of a dielectric prism, and the path of the beam is indicated. Several solutions can be derived from it, as discussed in the text. In the left bottom of the picture a graphical representation of the optical properties of the central beam splitter. Each thick arrow is equivalent to a free propagation, while the thin ones represent a transmission or a reflection through the interface. Filled circles stand for the different representative values of the input (i_1, i_2, i_3, i_4) and output (o_1, o_2, o_3, o_4) fields.

detail. In the following we will study several options, trying to understand their advantages and their drawbacks. In Sec. II we describe their optical properties, we introduce a reference scheme for a Virgo-like, coatingless interferometer and we discuss resonating modes, polarization effects and losses.

In Sec. III we evaluate the thermal noise performances of coatingless solutions. As we said elimitation of coatings should give us an advantage in terms of the quality factor of the optical elements. However in our setup the beam's light propagates inside the dielectric for a larger than usual length, and its coupling to thermal fluctuations of the refraction index n [7] can be large and must be understood.

In Sec. IV we draw some conclusions and we discuss possible improvements.

II. THE OPTICAL SCHEME

To explain our strategy we start from the basic setup depicted in Fig. 2. The four external triangles represent reflectors of the kind discussed in B&V which act simply as a mirror on the centered beam. The central triangle is the section of a prism, which acts as a beam splitter. The beam impinges on the surface $\mathcal{S}$ with a non zero incidence angle α, and is partially reflected and partially transmitted. The transmitted part exits the prism through the surfaces $\mathcal{N}$ or $\mathcal{N}'$. Spurious reflected beams can be generated by the reflection on the $\mathcal{N}$, $\mathcal{N}'$ surfaces of the prism and on the frontal surfaces $\mathcal{F}_i$ of the reflectors. To avoid them the curvature of these reflecting surfaces must be matched to the equal phase profiles of incoming beam.

This scheme is not directly usable because there is not an input or output port. The basic idea is to remove one of the reflectors $\mathcal{R}_i$, $i = 1, 2, 3, 4$, and to study the properties of the obtained one port device to see if it can be used as a resonant cavity in a gravitational wave detector. As we will see when we remove one of the reflectors we end with a device which contain several coupled cavities. All these are potentially able to resonate. To obtain optical properties equivalent to the ones of a Fabry-Perot we must tune the parameters in such a way that only one of these will remain relevant.

A. Optical transfer function

We suppose that the setup can be designed in such a way to sustain a resonant mode. Here we are interested in understanding only the qualitative picture, so we will forgot the nature of these modes that will be discussed later, and we threat them simply as plane waves.

We start with a characterization of the simpler triangular reflector, giving the relation between the incoming and outgoing fields a_{out} and a_{in}. This is essentially a single ended cavity, so we have to evaluate the interference among the multiple reflections from the entry surface and the total internal reflection in the interior. Summing all the contributions it is immediate to write

$$a_{\text{out}} = \frac{(n-1) + (n+1)e^{i\Phi}}{(n+1) + (n-1)e^{i\Phi}} a_{\text{in}} \equiv e^{i\zeta} a_{\text{in}}, \tag{3}$$

where $\Phi = 2nh_i k + \delta$ is the phase acquired during a round trip, which include the contribution of the propagation in the dielectric and the (polarization dependent) phase shift of the reflection δ. It is easy to see that the effect of the reflector is, as expected, simply a frequency dependent phase shift of the field. The beam entering the reflector will contain the carrier field, of frequency ω_0, and sidebands at frequencies $\omega_0 + \Omega$ carrying informations about the modulations at acoustical frequencies Ω. Taking $h_i \simeq 10^{-1}$ m we get $\Omega h_i/c < 10^{-4}$, and the finesse of the cavity is quite low. This means that we can neglect the frequency dependence of the phase shift factor ζ. In other words the reflector is just equivalent to a coatingless mirror (CM).

The crucial object for the solution we propose is the central beam splitter in Fig. 2. As we said in order to avoid coupling to spurious modes through internal reflection its triangular geometry must be designed in such a way that the beams refracted by the surface $\mathcal{S}$ are orthogonal to the surfaces $\mathcal{N}$ and $\mathcal{N}'$, with a matched curvature. This means that the angle of incidence of the incoming beam must be planned in advance.

As a beam splitter the prism is a four port device. In the left bottom of Fig. 2 we introduced a graphical representation which describes its optical properties. Thick arrows are associated to free propagators (phase factors in our case) and thin ones to appropriate reflection and transmission coefficients for the amplitudes of the fields. The graphical representation is equivalent to a linear relation between input and output fields that can be parametrized with an array of dimension four. Using the conventions explained in the caption of Fig. 2 we can write

$$\begin{pmatrix} o_1 \\ o_2 \\ o_3 \\ o_4 \end{pmatrix} = \Delta^{-1}\Gamma \begin{pmatrix} i_1 \\ i_2 \\ i_3 \\ i_4 \end{pmatrix}, \tag{4}$$

where $\Delta = 1 - e^{4i\delta}R^2r^2$ is the factor connected to the resonance inside the beam splitter and $\Delta^{-1}\Gamma$ is an array constrained by the unitarity, the time reversal invariance and the simmetry of the system. The elements of the array Γ can be written explicitly in the form

$$\Gamma_{11} = \Gamma_{22} = -e^{2i\delta}nrT^2, \tag{5}$$

$$\Gamma_{12} = \Gamma_{21} = R(1 - r^2e^{4i\delta}), \tag{6}$$

$$\Gamma_{33} = \Gamma_{44} = r(1 - R^2e^{4i\delta}), \tag{7}$$

$$\Gamma_{34} = \Gamma_{43} = -e^{2i\delta}nRt^2, \tag{8}$$

$$\Gamma_{14} = \Gamma_{23} = \Gamma_{32} = \Gamma_{41} = e^{3i\delta}nrtRT, \tag{9}$$

$$\Gamma_{13} = \Gamma_{31} = \Gamma_{42} = \Gamma_{24} = e^{i\delta} ntT, \tag{10}$$

where R, T are the reflection and transmission coefficients on the $\mathcal{S}$ surface for a beam incoming from the vacuum side, r, t the same for the $\mathcal{N}$ surface and $\delta = knd$. As the incidence angle of the beam from the two sides of the surface $\mathcal{S}$ is not at the same angle a normalization factor proportional to the square root of the ratio between the transverse surfaces of the incident and transmitted beam is attached to T.

We can transform the beam splitter in the equivalent of a semitransparent mirror deactivating two of the four input and output ports. This can be done feeding an input port with the beam exiting an output one. In Fig. 2 for example each beam is reflected in itself. We could also reflect, for instance, o_3 in i_4 and o_4 in i_3, but we will not report the analysis of these possibilities here, which however do not seem to be particularly interesting.

1. Coatingless semitransparent mirrors.

Given the symmetries of the beam splitter there are four independent ways of building a coatingless semitransparent mirror (CSM).

The realizations of all the four schemes we will analyze are depicted in Fig. 3. The first option, which we call type I, is given by the connections $(o_1 \rightarrow i_1,\ o_4 \rightarrow i_4)$. The types II, III and IV can be obtained similarly with the connections $(o_3 \rightarrow i_3,\ o_4 \rightarrow i_4)$, $(o_1 \rightarrow i_1,\ o_3 \rightarrow i_3)$ and $(o_1 \rightarrow i_1,\ o_2 \rightarrow i_2)$.

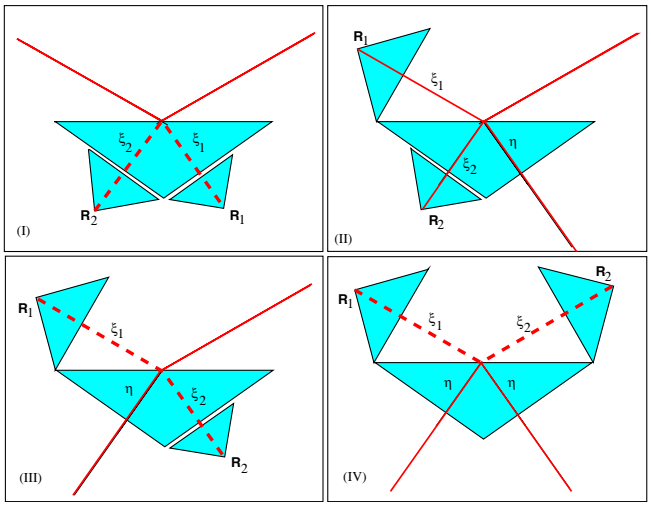

FIG. 3 (color online). The four schemes considered for a coatingless semitransparent mirror equivalent. Two reflectors are added to the beam splitter and used to reduce the number of input and output ports to two. Note that in some cases one or both of the added reflectors could be attached to the beam splitter, in order to obtain a monolithic object. A dashed line indicate a particular internal resonant path, see the text for a discussion.

Note that in Fig. 3 we consider the beam splitter and the "near" reflectors as separate objects. In a real setup it could be possible to merge one or both the reflectors with the beam splitter, obtaining a monolithic object which does not need to be aligned. For example, it is probably convenient to merge one of the reflectors in scheme I, II, III, while it could be difficult to do that in the scheme IV. Apart from the technical difficulties, the mechanical properties of the result will not be good, with elastic modes of low frequency and high disomogeneities of the mechanical stress. Of course the alignment of two separate pieces requires some kind of locking procedure. The scheme I could be in principle completely monolithic, but in that case it will not be possible to correct for imperfections in the manufacture.

We take as an example the case of scheme IV to show what is the general structure of the problem. First of all we can rewrite the relation (4) as

$$\begin{pmatrix} \mathbf{o}_u \\ \mathbf{o}_d \end{pmatrix} = \begin{pmatrix} \Lambda_{uu} & \Lambda_{ud} \\ \Lambda_{ud}^T & \Lambda_{dd} \end{pmatrix} \begin{pmatrix} \Xi \mathbf{o}_u \\ \mathbf{i}_d \end{pmatrix}, \tag{11}$$

where $\mathbf{o}_u^T = (o_1, o_2)$, $\mathbf{o}_d^T = (o_3, o_4)$, $\mathbf{i}_d^T = (i_3, i_4)$ and Λ_{ab} are the relevant 2×2 blocks of the array $\Delta^{-1}\Gamma$.

The diagonal array Ξ has elements proportional to the phase shifts acquired by the beam in a round trip from a surface of the beam splitter to a reflector:

$$\Xi_{ii} = e^{i\zeta_i + 2i\Phi_{\ell_i}} \equiv e^{i\xi_i}, \tag{12}$$

which is the sum of the contribution ζ_i of a reflector [see Eq. (3)] and of the free propagation over a length ℓ_i ($\Phi_{\ell_i} = k\ell_i$).

Solving we get the desired relations:

$$\mathbf{o}_u = (I - \Lambda_{uu}\Xi)^{-1}\Lambda_{ud}\mathbf{i}_d, \tag{13}$$

$$\mathbf{o}_d = [\Lambda_{dd} + \Lambda_{ud}^T \Xi (I - \Lambda_{uu}\Xi)^{-1}\Lambda_{ud}]\mathbf{i}_d \equiv \Lambda_{34}\mathbf{i}_d. \tag{14}$$

We are especially interested in Eq. (14), which gives the transfer functions between the two input $\mathbf{i}_d$ and output $\mathbf{o}_d$ ports of our CSM. The 2×2 array Λ_{34} must be unitary and, owing to time reversal invariance, symmetric. So its structure must be

$$\Lambda_{34} = e^{i\alpha} \begin{pmatrix} re^{i\beta} & t \\ t & -re^{-i\beta} \end{pmatrix}, \tag{15}$$

where the real parameters r and t represent the effective reflectivity and the transmissivity of the "mirror" and $r^2 + t^2 = 1$. Comparing Eq. (14) and (15) we can extract the reflectivity of this configuration. We can use the same method to prove that all the schemes represented in Fig. 3 represent a CSM and to evaluate their reflectivity. By adding a CM on one of the remaining port, at a large distance from the beam splitter, we can now build a resonant cavity which can be used to sense the gravitational strain, and finally a complete interferometer.

The transfer function of the cavity can always be written as

$$\text{out} = -e^{i(\alpha-\beta)}\frac{r - e^{i(\alpha+\beta+\zeta+2k_0\ell)}}{1 - re^{i(\alpha+\beta+\zeta+2k_0\ell)}}\ \text{in}. \tag{16}$$

This expression shows clearly that the the phase shifts α, β, ζ can be absorbed in a shift of the resonant length of the cavity, while the finesse is completely determined by the effective reflectivity r.

From Eq. (15) it follows that r depends on several factors. First of all there is a dependence from the incidence angle of the input beam on $\mathcal{S}$. This is because the transmission and reflection coefficients T and R enters inside the matrix elements of $\Delta^{-1}\Gamma$ and are incidence angle dependent. Another less obvious dependence is from the phase shifts inside the CSM. These phase shifts are practically not predictable, because it is not possible to manufacture a CSM with a precision in its geometrical parameters up to a fraction of the wavelength. In any case geometrical parameters (and the refraction index) are temperature dependent and will fluctuate. As a consequence in the general case both a phase noise and a fluctuation of the cavity's finesse will be introduced into the system.

It is possible however to tune the system and stabilize its fluctuations up to some extent. Two obvious possibilities are to change the temperature or the distance between the beam splitter and the near reflectors in Fig. 3. The last approach could be another motivation for keeping a reflector separated from the beam splitter. As we will see this gives us in principle a way of tuning the finesse of the cavity, a possibility which could have several interesting application.

2. Scheme I

We discuss in detail some peculiarities of the first scheme, which is the simplest one. The transfer function between the input and the output of this kind of cavity can be parametrized as

$$\mathcal{T}_I = e^{i(\alpha+\xi_2)}\frac{r - e^{i(\xi_1+\alpha+\phi)}}{1 - re^{i(\xi_1+\alpha+\phi)}}, \tag{17}$$

where the effective reflectivity is given by

$$r = \frac{1 - R^2}{\sqrt{1 + R^4 - 2R^2\cos\xi}} \tag{18}$$

and it is limited in the interval

$$\frac{1 - R^2}{1 + R^2} \le r \le 1. \tag{19}$$

Here ξ_i are the phase shifts in the two paths inside the CSM [see Fig. 3(a)], $\xi = \xi_1 + \xi_2$ and $\phi = k_0\ell + \zeta$. The phase α is defined by

$$e^{-i\alpha} = \frac{1 - R^2 e^{i\xi}}{\sqrt{1 + R^4 - 2R^2\cos\xi}}. \tag{20}$$

The transfer function in (17) is of the general form of Eq. (16) and for a fixed value of the parameters ξ_i is equivalent to the one of a simple Fabry-Perot cavity. A ξ_i's variation induces a shift in the resonant values of ϕ, a phase shift and a correction to the effective reflectivity r.

The maximum value $r = 1$ is obtained at $\xi = 0$, which correspond to the resonance of the path inside the CSM represented in Fig. 3(a) with a dashed line.

The minimum value of r correspond to the antiresonance $\xi = \pi$ and is plotted as a function of R in Fig. 4 (continuous line). Apparently there are two different possibilities of obtaining a high effective reflectivity, namely, we can tune the CSM on its internal resonance or we can choose a small value of R, which is related to the incidence angle θ_i. The minimal r is plotted as a function of θ_i in Fig. 5 and 6, respectively, for a polarization parallel and perpendicular to the incidence plane.

The more relevant feature is the clear peak $r = 1$ at the Brewster's angle (polarization parallel to the incidence plane, $R = 0$) which for SiO_2 is given by $\theta_{br} = 0.305\ \pi$ rad. Near this value the finesse of the cavity becomes very high.

To obtain the dependence of the finesse from the temperature we can write

$$\frac{1}{\mathcal{F}}\frac{d\mathcal{F}}{dT} = -\left(n\alpha + \frac{dn}{dT}\right)\frac{2\pi L}{\lambda}G(R, \mathcal{F}), \tag{21}$$

where

$$G(R, \mathcal{F}) = \frac{1}{\mathcal{F}}\frac{d\mathcal{F}}{dr}\frac{R^2(1 - R^2)\sin\xi}{[1 + R^4 - 2R^2\cos\xi]^{3/2}}, \tag{22}$$

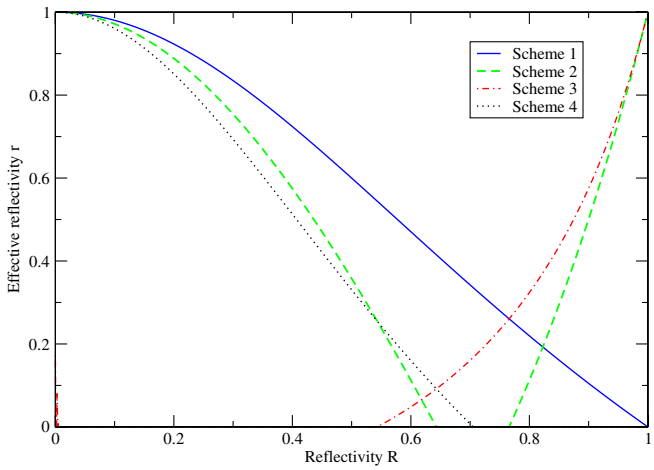

FIG. 4 (color online). The effective reflectivity r minimized over the phase shifts connected to the geometry in the four schemes analyzed. The reflection coefficient R on the surface $\mathcal{S}$ is on the horizontal axis. The reflectivity ρ is fixed to the value of SiO_2.

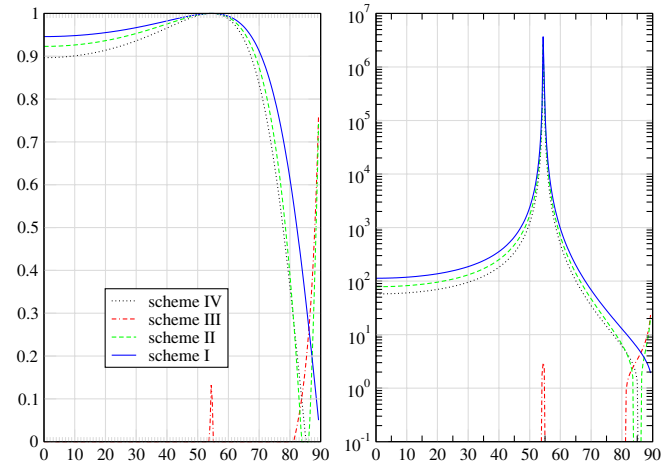

FIG. 5 (color online). On the left plot the effective minimum reflectivities as a function of the input beam's incidence angle on the beam splitter surface are compared among the different schemes. On the right plot we show the finesse of the corresponding single ended coatingless resonant cavity. Here $n = 1.42$ (silica) and the polarization is parallel to the incidence plane.

and the phase ξ can be expressed as a function of R and $\mathcal{F}$ using Eq. (18). Here we used the fact that a variation of temperature generate both a rescaling of the geometric lengths proportional to the linear thermal expansion coefficient α and a variation of the refraction index.

The relative temperature variation of the finesse is so given by a function $G(R, \xi)$, which is represented in Fig. 7, multiplied by a material dependent factor proportional to the ratio L/λ between the length of the path inside the CSM and the wavelength of the light in the vacuum.

For fused silica at 300 K this factor is dominated by the temperature dependence of the refraction index, and as a typical order of magnitude we get

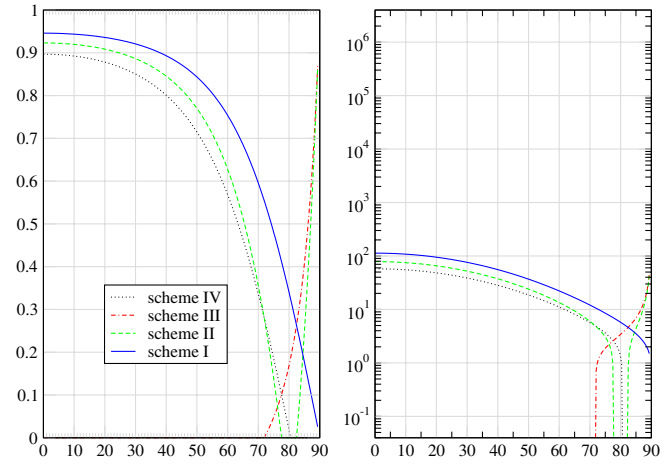

FIG. 6 (color online). The same of the Fig. 5 for a beam polarized perpendicularly to the incidence plane.

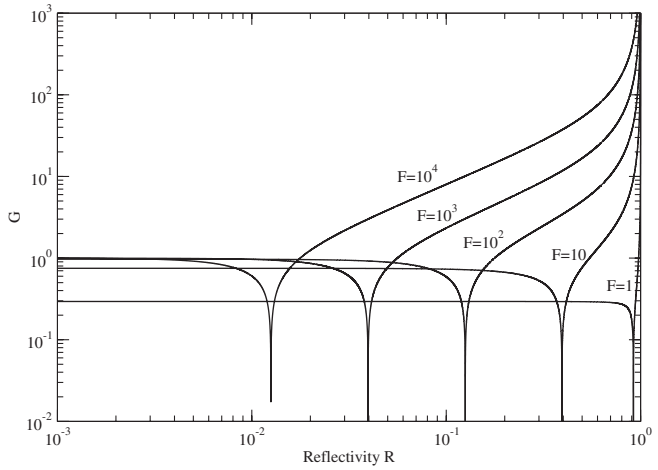

FIG. 7. The function $G(R, \mathcal{F})$ defined in Eq. (22). For a given value of the finesse R can be tuned in such a way to minimize $\mathcal{F}^{-1}\partial\mathcal{F}/\partial T$.

$$\left(n\alpha + \frac{\partial n}{\partial T}\right)\frac{2\pi L}{\lambda} \sim 95 \times \left(\frac{L}{1m}\right), \tag{23}$$

while for sapphire at 40 K

$$\left(n\alpha + \frac{\partial n}{\partial T}\right)\frac{2\pi L}{\lambda} < 6 \times \left(\frac{L}{1m}\right). \tag{24}$$

Figure 7 confirms that a given finesse $\mathcal{F}$ can be obtained for every incidence angle with an appropriate tuning of ξ. However in order to obtain an acceptable temperature stability for large values of $\mathcal{F}$ we are forced to choose a low reflectivity R, which means an incidence angle near the Brewster's one.

The best solution from the point of view of thermal stability is to choose as a working point, for a given value of $\mathcal{F}$, the incidence angle which correspond to the zero of G. This is the $\xi = \pi$ case, because as we saw the finesse has a miminum there and so does not change with ξ up to the linear order [Eq. (18)].

Of course we need a procedure to lock the apparatus both on this point and on the resonance of the "long" cavity. As we are trying to control two different degrees of freedom we need two independent error signals. The first one, which we call ε_1, can be obtained with the usual Pound Drever technique applied to the reflected input field. Introducing a modulation frequency ϖ we can write

$$\varepsilon_1 = \arg[2\mathcal{T}_I(\omega) - \mathcal{T}_I(\omega + \varpi) - \mathcal{T}_I(\omega - \varpi)], \tag{25}$$

which is zero when the phase at the carrier frequency is equal to the mean of the phase at the two sidebands. A typical modulation frequency will be lower than the free spectral range of the long cavity, $\varpi < c/L$. On this scale the variation of the phase shifts α, ξ_i is very small, and we can neglect the small offset they introduce. The zero of the error signal ε_1 obtained will be at $\phi + \xi_1 + \alpha = 0$, the resonance condition for the long cavity.

We consider now the field amplitude on the reflector R_2. We get the expression

$$u_2 = \frac{T(1 - e^{i(\phi+\xi_1)})}{1 - (1 - R^2)e^{i(\phi+\xi_1)} - R^2 e^{i\xi}} in, \tag{26}$$

which goes to zero when $\phi + \xi_1 = 0$. In this condition the phase of the light on the output port is unaffected by a movement of the reflector R_2. We define the second error signal to be $\varepsilon_2 = \phi + \xi_1$.

Locking on both ε_1 and ε_2 we get $\alpha = 0$, which correspond to $\xi = \pi$. We want to stress again that choosing this working point we obtained both a strong stabilization of the cavity finesse (temperature independent up to the linear order in the fluctuations) and a decoupling of the system from position of R_2.

An interesting possibility is to add an offset to the error signal ε_2. In this way we should be able to lock the system on the resonance of the long cavity, but at a tunable value $\xi = \pi + \delta$, which means a tunable value of the cavity finesse. Of course in this case a linear coupling between temperature and finesse is reintroduced, together with some sensitivity to R_2 displacement. To evaluate this in a more quantitative way we evaluated some derivatives of the output phase. The first one, expanded to the second order in δ, is

$$\frac{d\phi_{\text{out}}}{d\phi} \simeq -\frac{1}{R^2}\left(1 + \frac{1 - R^2}{4(1 + R^2)}\delta^2\right) \tag{27}$$

and give us informations about the variation of finesse with δ. The second is

$$\frac{d\phi_{\text{out}}}{d\xi_2} \simeq -\frac{1 - R^2}{4(1 + R^2)^2}\delta^2, \tag{28}$$

which give us a measure of the R_2's fluctuations reintroduced. One important point is that R_2's fluctuations are not amplified by the finesse of the cavity, so that their reintroduction is acceptable.

3. Scheme II

This scheme is equivalent to a Michelson interferometer with a small power recycling induced by the normal reflection on the CSM. We write directly the effective reflectivity which is given by

$$r = \left| \frac{\rho - R^2 e^{i(2\eta+\xi_1)} - (1 - R^2)e^{i(2\eta+\xi_2)}}{1 - \rho R^2 e^{-i(2\eta+\xi_1)} - \rho(1 - R^2)e^{-i(2\eta+\xi_2)}} \right|, \tag{29}$$

where $\rho = (n - 1)/(n + 1)$ is the reflection coefficient on the dielectric at a normal incidence angle and ξ_i, η the phase shifts defined in Fig. 3(b). In this case r is limited in the interval

$$\max\left(0, \frac{1 - \rho - 2R^2}{1 - \rho + 2\rho R^2}, \frac{2R^2 - 1 - \rho}{1 + \rho - 2\rho R^2}\right) \le r \le 1. \tag{30}$$

We obtain $r = 1$ if $\xi_1 = \xi_2$, which can be understood as the dark fringe condition for the equivalent Michelson.

Looking at Fig. 4 we see that for lower values of the reflectivity R the situation is quite analogous to the one of the previous case. On the contrary at higher values of R the minimal effective reflectivity start again to increase. However this range of R values correspond to incidence angles very near to $\pi/2$ (as can be seen looking at Fig. 5 and 6) which are quite unpratical.

4. Scheme III

This case is quite different from the others. The effective reflectivity can be written as

$$r = \left| \frac{\rho - \rho(1 - R^2)e^{i(\xi_1+\xi_2)} - R^2 e^{i(2\eta+\xi_2)}}{1 - (1 - R^2)e^{-i(\xi_1+\xi_2)} - \rho R^2 e^{-i(2\eta+\xi_2)}} \right| \tag{31}$$

with

$$\max\left(0, \frac{R^2 - \rho(2 - R^2)}{2 - R^2 - \rho R^2}\right) \le r \le 1. \tag{32}$$

Total reflection is obtained when $\xi_1 + \xi_2 = 0$, which is the resonance condition for the dashed path in Fig. 3(c).

From Fig. 4 we see that the minimal reflectivity is high only for high values of R, which as we said in the previous section are not convenient for a practical implementation.

5. Scheme IV

We do not report the explicit formula for the effective reflectivity, which is bounded in the interval

$$\max\left(0, \frac{(1 - \rho)^2 - R^2(1 + \rho)^2}{(1 - \rho)^2 + R^2(1 + \rho)^2}\right) \le r \le 1. \tag{33}$$

This scheme is quite similar to the first one, with a high minimal effective reflectivity near the Brewster's incidence angle (see Fig. 4).

6. General discussion

A first observation is that in all the cases considered with an appropriate tuning of the phase shifts δ, ξ_i it is always possible to set the effective reflectivity between 1 and a minimal value which is determined only by the incidence angle and the refraction index [Eqs. (19), (30), (32), and (33)].

The maximal reflectivity (total reflection) correspond to a resonant path inside the CSM in schemes I, III, IV (evidenced with a dashed line in Fig. 3) and to a total destructive interference in the Michelson-like scheme II. The minimal reflectivity, which is the more stable point, is analogously connected to an antiresonant path or to a completely constructive interference.

We want to discuss now the effect of the incidence angle. The reflectivity R is a function of the polarization, so we need to deal separately with two different cases. In Fig. 5 we plotted the minimal effective reflectivity (left side) and

the related finesse of a cavity built with a CSM, for a polarization parallel to the incidence plane.

The main feature is the evident peak around the Brewster's angle. The results for a polarization perpendicular to the incidence plane are shown in Fig. 6. Note that in this case there is no a Brewster's angle and the reflectivity R never goes near one.

It should be observed that a very large incidence angle is not convenient. In that case in order to accomodate incoming beams without losses we are forced to increase the size of CSM. Large incidence angles means also unavoidable distortion effects.

A small incidence angles is neither convenient. Also in this case a large CSM is needed, this time to allow a good separation of the two beams refracted inside the material.

From this point of view schemes I, II, IV are more or less equivalent. In each of them if high finesses are desired the incidence angle can be set near the Brewster's one, choosing the appropriate polarization. Scheme III is the only one which couples the cavity through a transmission, and apparently is much less convenient.

We see that schemes I, III, IV have a very similar behavior, with a pronounced maximum of the minimal reflectivity at an incidence angle α which is the Brewster's one. Here $R \rightarrow 0$ and the finesse of the cavity is nominally infinite, and cannot be tuned.

B. A "real" optical scheme

As we saw there are several ways to implement a CSM. In this section we will discuss in a more detailed way a complete optical scheme for a ''Virgo-like'' interferometer. This is depicted in Fig. 8. The interferometer is built using two equivalent Fabry-Perot like cavities which are kept in resonance. The light is fed inside through the ''light port'' LP, and is split and recombined by the conventional beam splitter BS.

For definiteness the prisms $P_{1,2}$ used to build the cavity are of the type I discussed in Sec. II.

1. Ideal cavity modes

We give now a simple discussion of the Gaussian resonating modes inside the cavity, in the paraxial approximation. Detailed calculations, which are quite standard, are omitted.

To describe the Gaussian mode we can introduce the usual complex parameter q defined by [8]:

$$\frac{1}{q} = \frac{1}{\rho} - i\frac{\lambda}{\pi w^2}, \tag{34}$$

where ρ is the curvature radius of the beam's phase front and w its transverse width, both evaluated at a reference position. To determine the q of the resonant mode we could represent the possible optical paths of the beam inside the cavity using a diagram similar to the one in the left bottom of Fig. 2. The action of an $ABCD$ optical matrix M on the q parameter is given by

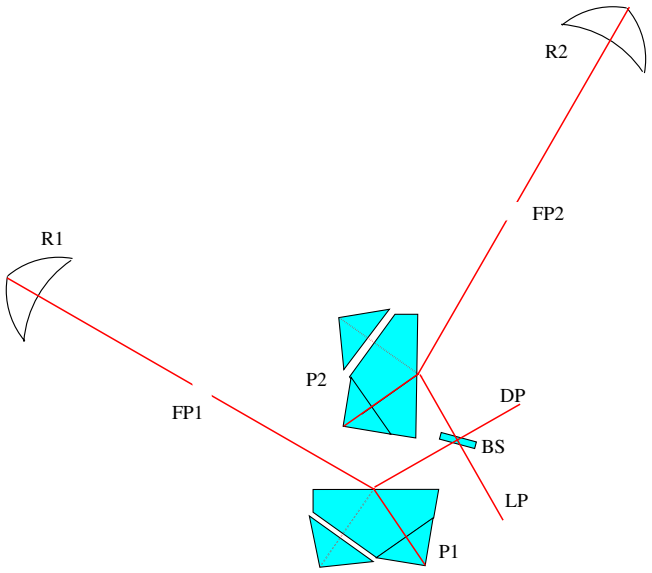

FIG. 8 (color online). The scheme of a Virgo-like, coatingless interferometer. The equivalent of the long Fabry-Perot cavities $FP_{1,2}$ are obtained here using a reflector R_i and a type I CSM P_i. The CSM depicted here is not completely monolithic, see the text for a discussion.

$$q' = \frac{M_{11}q + M_{12}}{M_{21}q + M_{22}} \equiv Mq \tag{35}$$

and that we can write the optical matrix which correspond to an arbitrary path on the diagram. In this way given q on a particular point on the graph we can evaluate it in all the other points simply propagating it with the appropriate matrix.

If, as in our case, there are closed loops, self consistency requires propagations along different paths to be equivalent. For a single closed loop represented by a round trip operator G this is just the constraint which determine the parameters of the resonant mode:

$$q = Gq, \tag{36}$$

while in the general case an additional number of conditions must be satisfied.

For a systematic study we could exploit all the relations represented graphically in the diagram. A simpler procedure can be described as follows.

The idea is to change the order of reasoning, matching the apparatus to a desired Gaussian beam. We can put, for example, the beam's waist on the frontal surface of the CSM, setting

$$\frac{1}{q^*} = -i\frac{\lambda_0}{\pi n w_0^2}, \tag{37}$$

where λ_0 is the wavelength in the vacuum. This has the advantage that a matched CSM can be built with flat

surfaces. Another advantage is that the CSM can be kept relatively small without introducing optical losses, which is important because a large object could have low frequency elastic internal modes, and it is more difficult and expensive to build. On the other hand, a large beam's spot is connected to a reduction of thermal noise. This is particularly true for thermorefractive noise, which will be discussed in Sec. III.

Now we can propagate the mode using the appropriate matrix. When the beam meet an interface, we match its radius of curvature ρ with the surface's one. The result is that the profiles of incoming and reflected beams can be overimposed. In this way we obtain a standing wave mode inside the cavity, and we can calculate the beam parameter in each point.

If we choose to put the waist of the Gaussian mode on the CSM, we need to match both the front and the back surfaces of the reflector in order to obtain a stable cavity. The solution can be constructed starting from the idealized scheme depicted in Fig. 9. The reflector depicted has a back surface obtained joining the two rotation paraboloids described by the given equations. These paraboloids are used for convenience, but it is clear that any couple of surfaces which are matched up to the second order to these near the origin is equivalent in the paraxial approximation. By tracing the path of some ray we can derive the optical ABCD array which describe this system. By symmetry it is clear that they factorize in a block in the xz plane of the form

$$\begin{pmatrix} 1 & 0 \\ -2/L & 1 \end{pmatrix}$$

and in another one in the xy plane which differs only for the sign of the elements on the diagonal. This correspond to a spherical mirror of focal length $f = L/2$.

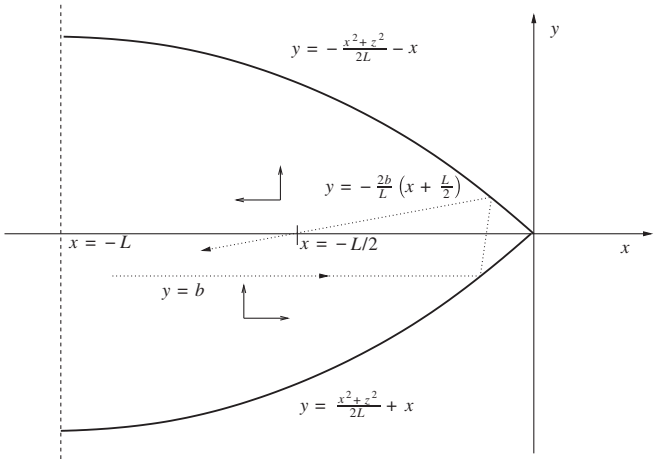

FIG. 9. Geometrical construction for the curvature of reflectors. Dashed contours are sections of paraboloid (rotation simmetry around the y axis). From this geometrical construction we can see that the reflector is equivalent to a mirror with a given radius of curvature.

2. Polarization effects

The optical properties of the proposed setup depends from the polarization of the beam [9]. This dependence is originated by two independent effects.

First of all the transmission and reflection coefficients, for a given non normal incidence, are different for polarizations parallel or perpendicular to the incidence plane. A general polarization is neither left invariant by reflection on the back surfaces of the reflectors and of the CSMs.

As a consequence a beam with a general polarization will not give a standing resonant wave inside the cavity. It is however possible to choose eigenstates of polarization which are able to resonate in the standard way. These eigenstates will depend on the relative orientation of the edges of the reflectors. With the simple setup depicted in Fig. 2 with parallel edges by symmetry considerations we can conclude that the eigenstates will correspond simply to a polarization vector parallel or perpendicular to the page.

We think that these polarization effects could be exploited to obtain control signals useful for the alignment of the apparatus. However we will not elaborate further on this point in this paper.

3. Light losses and misalignments

Several sources of light losses relevant for reflectors was discussed in B&V. These estimates can be applied also to the case of a CSM. Here we want only to add a couple of comments.

Diffraction effects on the edges of the reflectors could be reduced or eliminated using an intensity profile of the beam which is zero, together with its first derivative, on the edge. The simpler possibility is to use a superposition of a TE_{00} and a TE_{02} mode. However we have to be sure that the two modes will resonate inside the cavity at the same time, which will be the case if the Gouy phases of the two modes in a round trip differ by a multiple of 2π ($\psi_{\text{Gouy}} = \pi/2$). This can be achieved locating the waist of the beam at one of the mirrors of the cavity. In this configuration all Hermite modes TE_{lm} with even $l + m$ can resonate, so special care must be used to couple the cavity to the source. We expect also an increased sensitivity of the system to misalignments, though all resonant modes are not coupled at the lower dipole order.

Losses can arise because of distortions of a Gaussian beam when it is reflected or refracted by an interface. This effect could be estimated using a decomposition in plane waves of the incoming Gaussian beam. As each component is reflected or refracted it gets a different multiplicative factor so that the reconstructed beam is different from the expected Gaussian one. Losses can be evaluated comparing the reflected or refracted Gaussian beam with the one naively expected. In particular, if the beam is incident near

the total reflection angle some of the plane wave components can be transmitted and lost.

A study of the effect of misalignment on a reflector has also been done in B&V. The effect of the misalignment of a CSM can be estimated analogously using the well known techniques of modal expansion and perturbation theory.

We end this section with a comment on the effect of a wrong expose angle $\alpha \neq \pi/4$ of a CM, also discussed in B&V. We can see this as a perturbation which introduces couplings between Gaussian modes. But from another point of view this we can look at a cavity built with reflectors with arbitrary values of α. The non Gaussian modes which appears in this problem were studied in [10]. Here it was shown that resonant modes exists, and that this kind of cavities are always stable. We think that this is an interesting possibility to explore, and we are planning to do that in future.

III. THERMAL NOISE PERFORMANCES

There are several generation mechanism for thermal noise that have been studied extensively in the literature. In order to understand the advantages of a coatingless mirror we can discuss a set of quantities which give a measure of the importance of noises associated with the coating. Parameters used for numerical estimates are listed in Table I

An important parameter is the ratio $R_{\rm br}$ between the power spectrum of the Brownian noise associated with the coating with the one associated with the bulk. When $R_{\rm br} > 1$ we expect an improvement in Brownian's thermal noise amplitude associated with the elimination of coating. If the Young's modulus of the bulk is not too different from the one of the coating we can write

$$R_{\rm br} \sim \sqrt{\frac{d}{r_0(1-\sigma^2)}\frac{\phi_{\rm coat}}{\phi_{\rm bulk}}}, \tag{38}$$

where $\phi_{\rm bulk}$ is the bulk's loss angle and $\phi_{\rm coat}$ the one associated with the coating. From Eq. (38) it follows that $\phi_{\rm bulk}$ must be compared with $\phi_{\rm coat}$ times a diluition factor which is equal to the ratio between the width of the coating (typically $d \sim 10n^{-1}\lambda$) and the laser spot radius r_0 (some centimeters).

An analogous parameter can be written for the thermoelastic contribution,

$$R_{\rm th} \sim \frac{\alpha_{\rm eff}}{\alpha}\frac{d\sqrt{r_0}}{r_t^{3/2}}, \tag{39}$$

where $\alpha_{\rm eff}$ is the effective thermal expansion coefficient for the coating (for a Ta_2O_5/SiO_2 coating $\alpha_{\rm eff} = 1.8 \times 10^{-6}$ K^{-1}, see [11] for explicit expressions) and α the one of the bulk material. The thermal diffusion length is defined by

$$r_t = \sqrt{\frac{\kappa}{2\pi f \rho C_v}} \tag{40}$$

and sets the scale that must be compared with $(d^2 r_0)^{1/3}$. We see that the effect of coating becomes dominant when r_t is small. For thermorefractive noise, which is the one generated by the fluctuation of the refraction index, we get a similar formula

$$R_{\rm tr} \sim \frac{1}{\sqrt{\eta}}\frac{\beta_{\rm eff}}{\beta}\frac{\lambda\sqrt{r_0}}{r_t^{3/2}}, \tag{41}$$

where η is a geometrical scale factor which connect r_0 with the length of the optical path of the material inside the material, $r_0 = \eta\ell$. We expect typically $\eta < 10$. In Eq. (41) $\beta = dn/dT$ for the bulk material, and $\beta_{\rm eff}$ is an effective value of the same quantity for the coating (see Eq. 20 of [11]).

We can start now to discuss a "standard" scenario for a coatingless optics. In Fig. 10 we plot the equivalent strain amplitude for several different thermal noise contributions, in the case of a fused silica optics with $T = 300$ K.

The dominant source of thermal noise above 50 Hz is the Brownian one, and with the choosen parameters $R_{\rm br} \sim 2.5$ which is consistent with the observed importance of coating contribution. The thermal diffusion length is $r_t \sim 3.10^{-4} f^{-1/2}$ that compared with $(d^2 r_0)^{1/3} \sim 10^{-4}$ correctly predict the dominance of thermoelastic coating effects above few hertz. The relevant scale for thermorefractive noise is $(\lambda^2 r_0/\eta)^{1/3} \sim 4 \times 10^{-3}/\eta^{1/3}$ which agrees with dominant coating effects above 10^2 Hz.

TABLE I. Bulk physical parameters used in the extimations. For the estimation of coating effects we used $\phi_c = 10^{-4}$, $\alpha_{\rm eff} = 2.4 \times 10^{-6}$ K^{-1} and $\beta_{\rm eff} = 3 \times 10^{-5}$ K^{-1}. Values without reference are extrapolations.

Parameter	Notation	Unit	Fused Silica 300 K	Sapphire 300 K	Sapphire 10 K
Refraction index temperature coefficient	β	K^{-1}	-1.5×10^{-5} [11]	1.3×10^{-5} [12]	$\leq \lvert 9 \times 10^{-8} \rvert$ [12]
Absorption coefficient	ϵ	ppm cm^{-1}	2–20 [12]	40–100 [12]	90 [12]
Thermal conductivity	κ	W/mK	1.4 [11]	40 [11]	4×10^3 [12]
Linear expansion coefficient	α	K^{-1}	5.5×10^{-7} [11]	5×10^{-6} [11]	5.8×10^{-10} [23]
Loss angle	ϕ		5×10^{-9} [11]	3×10^{-9} [11]	3×10^{-10}
Specific heat	C	J/KgK	670 [11]	790 [11]	8.9×10^{-2} [23]
Young's modulus	E	Pa	7.2×10^{10} [11]	4×10^{11} [11]	4×10^{11}

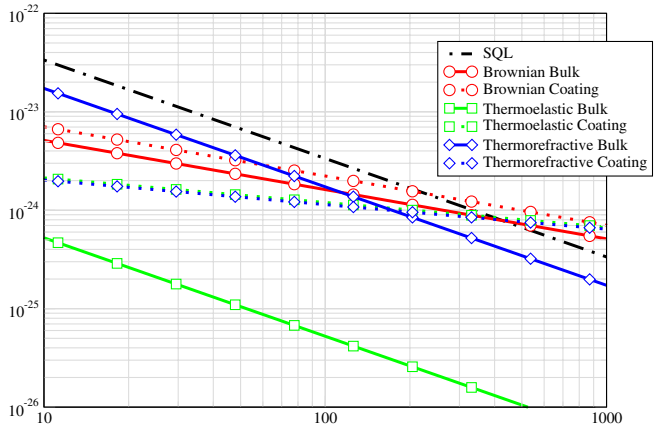

FIG. 10 (color online). Contributions to the thermal noise amplitude for fused Silica 300 K. On horizontal axis the frequency, on the vertical one the equivalent strain amplitude of the noise, in unit $Hz^{-1/2}$.

Looking at the absolute values of the various contributions we see that the introduction of a coatingless solution produce a modest improvement of the sensitivity above 80 Hz. Below this frequency the thermorefractive noise becomes dominant and the sensitivity is reduced.

The ratio between bulk thermorefractive and bulk Brownian noise amplitudes is given by

$$\sqrt{\frac{2E\eta}{(2\pi)^{3/2}(1-\sigma^2)f}}\frac{\kappa T}{\phi}\left(\frac{\beta}{\rho C_v r_0}\right), \tag{42}$$

which must be lowered in order to increase the advantages of a coatingless solution. One possibility is obviously to increase r_0 as much as possible, which is always a good practice for thermal noise reduction. When r_0 grows $R_{\rm br}$ decreases, which means that the coating noise becomes less important until there is no more an advantage in coating elimination. This will happen when $r_0 \sim d\phi_{\rm coat}/\phi_{\rm bulk} \sim 0.3$ m which practically is a quite large value. We think that the final message is that the improvement of a coatingless solution must be evaluated after r_0 being fixed to the largest value achievable.

Another option is to find a better material. The more direct approach is to reduce the optothermal parameter β. The Lorentz-Lorenz formula

$$\frac{n^2-1}{n^2+2} = \frac{\rho(T)\alpha_p(\rho,T)}{3\epsilon_0} \tag{43}$$

connect the refraction index to the density ρ and the polarizability α_p of the material. Evaluating the temperature derivative

$$\beta = \frac{(n^2-1)(n^2+1)}{6n}\left[\frac{1}{\alpha_p}\frac{\partial\alpha_p}{\partial T} - 3\alpha\left(1+\frac{\rho}{\alpha_p}\frac{\partial\alpha_p}{\partial\rho}\right)\right] \tag{44}$$

we see that there is a negative contribution to β connected to the thermal expansion of the material, and another one (which usually is positive) due to the intrinsic dependence of polarizability from the temperature. The linear expansion coefficient of fused silica is quite small ($\alpha \sim 0.5 \times 10^{-6}$ K^{-1}) and β is dominated by the temperature dependence of polarizability.

The situation is different for sapphire. The β value at $T = 300K$ is similar to the one of fused silica. The noise budget for this case is plotted in Fig. 11. We see that in this case we are entirely dominated by thermorefractive noise. There is 1 order of magnitude increase in the relative importance of thermorefractive versus Brownian bulk noise [Eq. (42)] which is due partly to the higher thermal conductivity and partly to the higher Young's modulus of Sapphire.

The ratio between thermorefractive and thermoelastic contributions of the bulk is given by

$$\frac{1}{(2\pi)^{1/4}}\left(\frac{\beta}{\alpha}\right)\frac{\sqrt{\eta}}{1+\sigma} \tag{45}$$

and is reduced by 1 order of magnitude, mainly for the increased linear expansion coefficient of Sapphire.

A very low upper limit for β was found at cryogenic temperature [12], and good performances for a coatingless interferometer could be expected in this regime. In Fig. 12 the estimate for different thermal noise amplitudes for sapphire at $T = 10$ K is plotted using that upper limit. In spite of the low β value thermorefractive noise is largely dominant. The reason is that at cryogenic temperature the specific heat of Sapphire becomes small (and the thermal conductivity increases). This largely compensate the improved optothermal coefficient and the explicit temperature factor.

The general conclusion seems to be that thermorefractive noise has a bad behavior in the low temperature

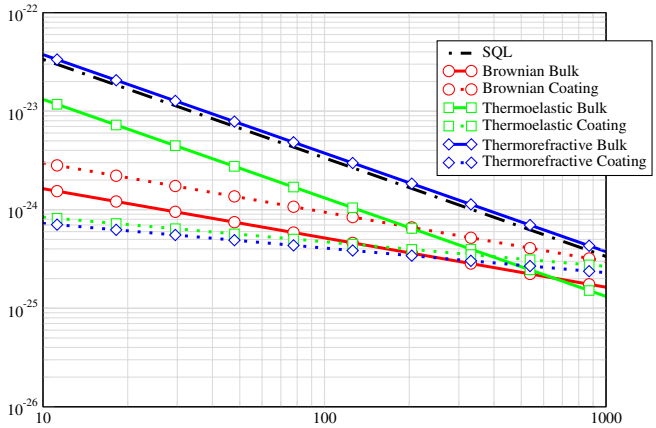

FIG. 11 (color online). Contributions to the thermal noise amplitude for Sapphire at $T = 300$ K. On horizontal axis the frequency, on the vertical one the equivalent strain amplitude of the noise, in unit $Hz^{-1/2}$.

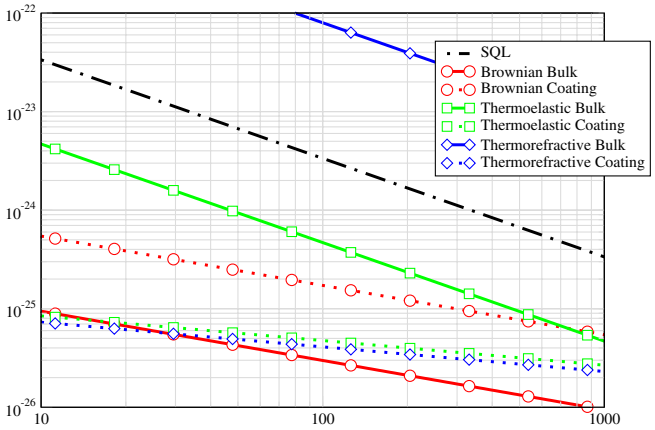

FIG. 12 (color online). Contributions to the thermal noise amplitude for Sapphire at $T = 10$ K. On horizontal axis the frequency, on the vertical one the equivalent strain amplitude of the noise, in unit $Hz^{-1/2}$.

regime: under the Debye's temperature $C_v \sim T^3$, while there are no reasons to expect a reduction of β [13–15].

On the other hand we could expect that, at least for materials with a not too small linear expansion coefficient, a cancellation between the two terms in the right side of Eq. (44) could occur for an appropriate temperature. We have no data to support this hypothesis, except the possible interpretation in this sense of the low β of Sapphire at cryogenic temperatures, but we think that it could be an interesting possibility to explore.

Finite size corrections

In the solution we propose light moves inside the dielectric material for optical lengths much larger than the usual ones. For this reason we expect that correlation and finite size effects could be more important that in the usual situation.

By traversing a dielectric material moving in the z direction between z_0 and z_1 a laser beam gets a phase shift which can be written as

$$\phi = k_0 \int_{z_0}^{z_1} dz \int dxdy n(x, y, z) I(x, y, z), \tag{46}$$

where k_0 is the wave vector of the beam, n the refraction index, which we suppose isotropic, and I the intensity profile of the beam, normalized in such a way that its integral over the transverse coordinates x, y is equal to one.

In a concrete scenario the beam will enter in the dielectric traversing an interface, and this will induce other contributions to the phase fluctuation. As a simplified case we look at a beam which traverse a dielectric slab of thickness ℓ, perfectly reflective on the other side. As usual the reflected beam can be written as

$$E_r = e^{i\phi_R + i\Xi} E_i, \tag{47}$$

where ϕ_R is the phase shift between a reference point and the first dielectric surface, and Ξ is the cavity phase shift, which is a function of the round trip phase ϕ_{RT} inside the slab. Taking the fluctuating part we get

$$\delta\phi = \delta\phi_R + \gamma\delta\phi_{RT} \tag{48}$$

where the factor

$$\gamma = \frac{1 - r^2}{1 + r^2 - 2r\cos\phi_{RT}} \tag{49}$$

is connected to the resummations of all the round trips. We write the first fluctuating term in Eq. (48) as

$$\delta\phi_R = 2k_0 \int I(x, y) u_z(0, x, y) dxdy. \tag{50}$$

This is the usual expression for the phase shift induced by a moving mirror, which is associated to the well studied Brownian and thermoelastic noise.

The second term can be written as a sum of two pieces, $\delta\phi_{RT} = \delta\phi^n_{RT} + \delta\phi^\ell_{RT}$, with

$$\delta\phi^n_{RT} = 2k_0 \int_0^\ell dz \int dxdy I(x, y) \delta n(x, y, z) \tag{51}$$

and

$$\delta\phi^\ell_{RT} = 2k_0 n|_{z=0}^{z=\ell} \int I(x, y) u_z(z, x, y) dxdy. \tag{52}$$

The term $\delta\phi^n_{RT}$ is connected to the intrinsic fluctuations of the refraction index. This can be seen simply as a phase shift induced by the fluctuation of the refraction index in each each volume element averaged with a weight proportional to the beam intensity.

The term $\delta\phi^\ell_{RT}$ takes into account the variation of the length of the slab and is of the same form of the mirror contribution in Eq. (50). The total power spectrum density of the phase noise can be written at the end as

$$\begin{aligned} S_\phi = {} & S_{\phi_R} + \gamma^2 (S_{\phi^n_{RT}} + S_{\phi^\ell_{RT}} + 2C_{\phi^n_{RT}, \phi^\ell_{RT}}) \\ & + 2\gamma (C_{\phi_R, \phi^n_{RT}} + C_{\phi_R, \phi^\ell_{RT}}), \end{aligned} \tag{53}$$

where C_{ϕ_1, ϕ_2} is the cross correlation spectrum between the fluctuations ϕ_1 and ϕ_2. We can conclude that a CM will be affected by all the noise sources of a conventional mirror without coating effects, and additionally by the noises induced by the fluctuation of the refraction index (the thermorefractive contribution).

The Eq. (53) expression shows that it is not legitimate to neglect the correlations between different kind of fluctuations summing the power spectral densities. This is really important of course only when the different fluctuations have the same order of magnitude, as it is expected for ϕ^ℓ_{RT} and ϕ_R. In these cases we cannot use blindly the expressions for Brownian and thermoelastic noise found in literature. The appropriate generalization can be obtained starting from the results of [16]. In this work an approxi-

mate but accurate solution for the elastic displacement induced on a cylinder by a pressure applied on its front face is determined.

It is easy to extend this to our case, where the pressures are on both faces. We consider for simplicity a cylinder with infinite radius and heigth ℓ, which admit an exact solution for the elastic displacements discussed in Appendix A. From this solution the relevant power spectral densities of thermal noise can be evaluated.

A more detailed study of the effect of noise correlations and finite size effects will be published elsewhere [17].

IV. CONCLUSION

In this paper we proposed a way to build high finesse resonant cavities without reflective coatings, solving the problem of laser injection and extraction. There are several different schemes, based on partial or total reflection on dielectric surfaces. In each case the finesse of the cavity is limited only by optical losses. Another advantage of our approach is that it is in principle possible to tune the cavity's finesse, which can be important, for example, to design an easy locking strategy but above all to match the two Fabry-Perot interferometer's cavities improving its sensitivity.

Thermal noise can be reduced owing to the higher quality factor obtainable in absence of reflective coating. We study two possible scenarios. In the first we use fused silica mirrors at ambient temperature, and we find a modest improvement of the sensitivity above 80 Hz. In the second we consider sapphire mirrors, bot at ambient and cryogenic temperature. In each case we found a noise dominated by the thermorefractive contribution, especially in the cryogenic regime, and a worsening of the performances compared with the standard solution with coatings.

The possibility of better results depends mainly on the reduction of thermorefractive noise, and we suggest the possibility of finding materials with very low values of the optothermal coefficient β at appropriate temperatures. Material with low Debye's temperature could also give some improvement in the cryogenic regime.

As the length of the optical path in our solution is much larger than the usual one there are two other effects which could reduce the sensitivity. The first is photo-thermal noise, a fluctuation of the mirror triggered by a direct absorption of a photon. Low values of β helps also in reducing this problem, together with low absorption coefficients. The second is thermal lensing, which is also proportional to absorptions and to the combination $\alpha\beta/\kappa$. Both effects depends on the power inside the cavity, and was not analyzed here.

We find a reasonable scenario in which the sensitivity can be improved, though by a not too large factor. What we get is a working alternative solution which avoid the use of coatings, and that could possibly be improved with a careful investigation of materials. Its practical feasibility depends mainly on the possibility of manufacturing dielectric prisms with material and interfaces of very high quality. An alternative approach for the reduction of coating's effects has been suggested in [18].

APPENDIX A: ELASTIC DISPLACEMENT OF AN INFINITE SLAB

In order to evaluate thermal noise spectra using the fluctuation dissipation theorem [19,20] we are interested to evaluate the elastic displacement of a dielectric slab (thickness ℓ) under the action of a pressure distributed on both sides. We assume a cylindrical symmetry for the problem: in this case it can be shown that the displacements can be written as [21]

$$u_r = \int_{-\infty}^{\infty} \left[\alpha + \left(kz - \frac{\lambda + 2\mu}{\lambda + \mu} \right) \beta \right] e^{-kz} J_1(kr) k dk, \quad (54)$$

$$u_z = \int_{-\infty}^{\infty} \left[\alpha + \left(kz + \frac{\mu}{\lambda + \mu} \right) \beta \right] e^{-kz} J_0(kr) k dk. \quad (55)$$

This correspond to the Eqs. 5 and 6 of Ref. [16], with the integration extended to negative values of k, which can be allowed owing to the finite thickness of the slab. From this expression the components of the stress tensor can be evaluated, obtaining

$$\sigma_{rz} = 2\mu \int [\beta - (1 + kz)\alpha] e^{-kz} J_1(kr) k^2 dk, \quad (56)$$

$$\sigma_{zz} = -2\mu \int [\alpha + \beta kz] e^{-kz} J_0(kr) k^2 dk. \quad (57)$$

Setting the boundary conditions at $z = 0$ and $z = -\ell$ we obtain the coefficients

$$\alpha = \frac{\tilde{p}_+ + e^{k\ell}(1 - k\ell + k^2\ell^2)\tilde{p}_-}{2k\ell \cosh k\ell - 2(1 + k^2\ell^2) \sinh k\ell} \quad (58)$$

and

$$\beta = \frac{(1 + k\ell)\tilde{p}_+ + e^{k\ell}(k^2\ell^2 \coth k\ell + 1 - k\ell)\tilde{p}_-}{2k\ell \cosh k\ell - 2(1 + k^2\ell^2) \sinh k\ell}, \quad (59)$$

where the functions $\tilde{p}_\pm(k)$ are proportional to the Hankel transform of the pressure in the $z = \ell$ ($\tilde{p}_+$) and $z = 0$ ($\tilde{p}_-$) face,

$$\tilde{p}_\pm(k) = -\frac{1}{2\mu k} \int_0^\infty p_\pm(r) J_0(kr) r dr. \quad (60)$$

We are interested to a pressure distributed as

$$p(r) = \frac{2}{\pi w_0^2} \exp\left(-\frac{2r^2}{w_0^2} \right), \quad (61)$$

which gives simply

$$\tilde{p}(k) = \frac{1}{2\pi} \exp\left(-\frac{1}{8} k^2 w_0^2\right). \quad (62)$$

The two important quantities requested for the evaluation of the thermal noise using the fluctuation dissipation theorem are the total elastic energy (for the Brownian contribution) and the volume integral of the square gradient of the dilatation $\Theta = \vec{\nabla} \cdot \vec{u}$ (for the thermoelastic one [22]).

The total elastic energy can be valuated as the work done by the pressure:

$$U_{el} = 2\pi \int [p_-(r) u_z(r, -\ell) - p_+(r) u_z(r, 0)] r dr. \quad (63)$$

while the dilatation is given by

$$\Theta = -\frac{\lambda + 3\mu}{\lambda + \mu} \int_{-\infty}^{\infty} \beta e^{-kz} J_0(kr) k^2 dk. \quad (64)$$

[1] S. D. Penn *et al.*, Classical Quantum Gravity **20**, 2917 (2003).
[2] D. Crooks *et al.*, Classical Quantum Gravity **19**, 883 (2002).
[3] G. M. Harry *et al.*, Classical Quantum Gravity **19**, 897 (2002).
[4] N. Nakagawa, A. M. Gretarsson, E. K. Gustafson, and M. M. Fejer, Phys. Rev. D **65**, 102001 (2002).
[5] K. Numata, M. Ando, K. Yamamoto, S. Otsuka, and K. Tsubono, Phys. Rev. Lett. **91**, 260602 (2003).
[6] V. B. Braginsky and S. P. Vyatchanin, Phys. Lett. A **324**, 345 (2004).
[7] V. B. Braginsky, M. L. Gorodetsky, and S. P. Vyatchanin, Phys. Lett. A **271**, 303 (2000).
[8] H. Kogelnik and T. Li, Appl. Opt. **5**, 1550 (1966).
[9] D. L. Bobroff, Appl. Opt. **3**, 1485 (1964).
[10] G. Toraldo di Francia, Appl. Opt. **4**, 1267 (1965).
[11] V. B. Braginsky and S. P. Vyatchanin, Phys. Lett. A **312**, 244 (2003).
[12] T. Tomaru, Classical Quantum Gravity **19** 2045 (2002) (Proceedings of the 4th Amaldi Conference).
[13] Y. Tsay, B. Bendow, S. S. Mitra, Phys. Rev. B **8**, 2688 (1973).
[14] J. Matsuoka and H. Yamashita, J. Non-Cryst. Solids **135**, 86 (1991).
[15] William J. Tropf, Opt. Eng. (Bellingham, Wash.) **34**, 1369 (1995).
[16] F. Bondu, P. Hello, and J. Vinet, Phys. Lett. A **246** 227 (1998).
[17] G. Cella, A. Giazotto, and K. Numata (unpublished).
[18] F. Ya. Khalili, Phys. Lett. A **334**, 67 (2005).
[19] H. B. Callen and R. F. Greene, Phys. Rev. **86**, 702 (1952).
[20] Y. Levin, Phys. Rev. D **57**, 659 (1998).
[21] L. D. Landau and E. M. Lifshitz, *Theory of Elasticity* (Pergamon, New York, 1986).
[22] Y. T. Liu and K. S. Thorne, Phys. Rev. D **62**, 122002 (2000).
[23] M. Cerdonio, L. Conti, A. Heidmann, and M. Pinard, Phys. Rev. D **63**, 082003 (2001).